Spatially Resolved Observation of Dipole-Dipole Interaction between Rydberg Atoms

C. S. E. van Ditzhuijzen,[1] A. F. Koenderink,[2] J. V. Hernández,[3] F. Robicheaux,[3]
L. D. Noordam,[1] and H. B. van Linden van den Heuvell[1,*]

[1]*Van der Waals–Zeeman Institute, University of Amsterdam, Valckenierstraat 65, 1018 XE Amsterdam, The Netherlands*
[2]*FOM-Institute for Atomic and Molecular Physics, Kruislaan 407, 1098 SJ Amsterdam, The Netherlands*
[3]*Department of Physics, Auburn University, Alabama 36849-5311, USA*

We have observed resonant energy transfer between cold Rydberg atoms in spatially separated cylinders. Resonant dipole-dipole coupling excites the $49s$ atoms in one cylinder to the $49p$ state while the $41d$ atoms in the second cylinder are transferred down to the $42p$ state. We have measured the production of the $49p$ state as a function of separation of the cylinders (0–80 μm) and the interaction time (0–25 μs). In addition, we measured the width of the electric field resonances. A full many-body quantum calculation reproduces the main features of the experiments.

Transport of excitations by resonant interaction between dipoles is a ubiquitous phenomenon that is fundamental to a broad range of disciplines, ranging from life sciences to quantum computing. In biological systems resonant dipole-dipole interactions mediate the ultrafast energy flow in light harvesting complexes responsible for photosynthesis [1,2]. Dipole-dipole interactions between fluorophores, as first described by Förster [3], are now a workhorse tool in biological imaging to measure nanoscale distances [4]. Furthermore, manipulating the coupling between dipoles is essential to a diverse range of emerging fields. In nanophotonics coherent dipole-dipole coupling between carefully placed polarizable plasmonic nanoparticles is pursued as a tool to create ultrasmall optical circuits [5–8]. For realizing quantum computing proposals, understanding of, and full control over, both the dynamics and the spatial properties of coherent excitation transfer between quantum systems is a crucial step [9–13].

The range of length and time scales over which dipole-dipole coupling occurs is ultimately set by the magnitude of the dipole moments of the involved atoms, molecules, or quantum dots. Unfortunately, the resulting time scales for dipole coupling are ultrafast, while the length scales are very small. Resolving and manipulating the interaction both in time and space simultaneously is therefore extremely challenging. For instance, temporal quantum control over dipole-dipole coupling has been demonstrated on a femtosecond time scale, yet without spatial information on excitation transport [2]. Conversely, Hettich *et al.* have resolved coherent coupling over nanometer length scales using spectral properties of two resonant molecules. Inherently this spectroscopic experiment provided no insight in or control over the temporal dynamics [14]. Already for some time, it has been realized that the large dipole moments of Rydberg atoms promise to remove this limitation. Interactions between Rydberg atoms occur over length and time scales that are easily addressable in an experiment [11]. Observations of dipole-dipole coupling between Rydberg atoms so far have only probed spectro-

scopic and dynamical properties without direct control over the interatomic distances [15–21].

In the experiment presented in this Letter, we control the spatial separation between Rydberg atoms in two dimensions and study the dynamics of resonant excitation transfer by dipole-dipole interactions. Distinct Rydberg states are created from a magneto-optical trap (MOT) of Rb atoms by pulsed excitation using two independent focused laser beams (Fig. 1). Dipole-dipole coupling causes a transition of a Rydberg atom ($49s$) in one volume to a higher state ($49p$) and a simultaneous transition of an atom ($41d$) in the second volume to a lower state ($42p$). This transition occurs over separations of up to 50 μm, over 10 μs time scales.

Dipole-dipole interactions in Rydberg atoms can be induced by tuning two transitions into resonance using a static electric field. A transition in rubidium, which has particularly large transition dipole moments and a resonance at a low electric field ($\sim$0.4 V/cm), is

$$41d_{3/2} + 49s_{1/2} \leftrightarrow 42p_{1/2} + 49p_{3/2}. \qquad (1)$$

The resonant transition frequency is 33 GHz. The strength of the dipole-dipole interaction is given by
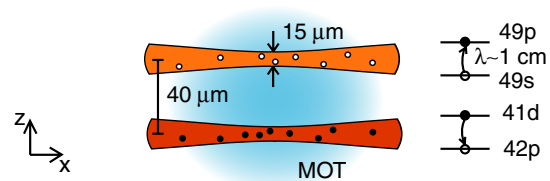

FIG. 1 (color online). Two pulsed laser beams excite cold atoms to Rydberg states. The $41d$ atoms in one volume interact with the $49s$ atoms in the other volume. The resonant dipole-dipole interaction giving rise to a change of states $41d + 49s \rightarrow 42p + 49p$ is in the near field limit ($R \sim 40$ μm $\ll \lambda = 0.9$ cm). We resolve the interaction in time and space by varying the beam separation.

$$V = \frac{\mu_1 \cdot \mu_2 - 3(\mu_1 \cdot \hat{\mathbf{R}})(\mu_2 \cdot \hat{\mathbf{R}})}{R^3}, \qquad (2)$$

where $\mathbf{R}$ is the distance vector between the interacting particles, μ_1 (μ_2) is the dipole moment of the $41d \rightarrow 42p(49s \rightarrow 49p)$ transition. Both dipole moments are of the order of $1000a_0e$. The transition probability $P \propto \sin^2(Vt)$ shows quantum beats with a period of ~14 μs for $R = 40$ μm (if $\mu_1, \mu_2 \parallel \mathbf{R}$). For short times ($Vt \ll 1$), we approximate $P \propto t^2/R^6$. For dipoles on parallel lines at distance d, the short-time probability averages to $P \propto t^2/d^5$.

The setup used is similar to [22] and consists of a standard ^{85}Rb MOT. The atoms hardly move on the time scale of the experiment as the average speed is below 0.3 μm/μs ($T = 300$ μK or less). The cold ground-state atoms ($5s$) are excited to a Rydberg state by an 8 ns laser pulse of 594 nm in a two-photon process. Two separate lasers, one for each of the two Rydberg states, are focused next to each other in the MOT cloud. The one that excites to the $49s$ state has a linewidth of 0.09(1) cm^{-1} and a pulse energy of 3.0(1) μJ. For the $41d$ laser we have 0.21(2) cm^{-1} and 5.0(1) μJ. The foci are imaged on a CCD camera, with a pixel size of 5.6 μm. The $49s$ beam can be laterally moved by a motorized lens.

An electric field surrounding the MOT cloud is created by applying a differential voltage on two 5.5 cm diameter circular plates, 2.5 cm apart, perforated by a 14 mm hole to allow MOT beams and ionization products to pass. This electric field, parallel to the laser beam separation and polarization, brings the dipole-dipole transfer [Eq. (1)] into resonance. After some interaction time an electric field pulse (from 0 to 150 V/cm in 5 μs) ionizes the atoms and the released electrons are detected by a microchannel plate (MCP). This gives different electron arrival times for the $49p$ and $49s$ atoms; the $41d$ and the $42p$ states are not distinguished. We use the $49p$ signal as a measure of the dipole-dipole interaction. Every electron is timed separately (the detection efficiency for MCP's is typically 40%–70%) and all data are averaged over 200 laser shots.

The initial number of measured $49s_{1/2}$ atoms per shot is 12.5(2.5) and the total number of atoms in the $41d$ volume is 70(10), not taking into account the MCP's finite detection efficiency. Of these atoms 15(3) are in the $43p$ state and we presume the same number in the $42p$ state. We get 24(5) atoms in the $41d_{5/2}$ state and 16(3) atoms in the relevant $41d_{3/2}$ state, based on the ratio given by our laser polarization. During the experiment, the number of Rydberg atoms slightly decreases due to spontaneous decay (rates around 8 kHz). Second, black body radiation induces transitions to nearby lying Rydberg states with rates around 10 kHz [23]. Reference measurements with an isolated $41d$ beam result in 0.5 $49s$ atom and 0.5 $49p$ atom and are subtracted from the data.

The Rydberg volumes are cigarlike ellipsoids. Their length is determined by the size of the MOT cloud (~0.5 mm). For unsaturated excitation we expect that the diameter of the Rydberg volume is $1/\sqrt{2}$ times the laser beam waist, because of the two-photon process. However, laser fluence dependent measurements show that both excitations are slightly saturated in our experiment, resulting in slightly larger diameters. The laser waists are determined by a two-photon overlap measurement. For this we detune the $49s$ laser by 20 GHz to the blue and we make sure that the laser pulses overlap in time, so that absorbing one photon of each laser leads to excitation to the $44d$ state. By moving the $49s$ beam over the $41d$ beam, one obtains the convolution of the two laser beams in the $44d$ signal. A measurement is depicted in Fig. 3 and fitted to a Gaussian profile with a $1/\sqrt{e}$ full width of 22.8(6) μm. Measurements as a function of saturation (not shown) yield a laser waist of 13.7(4) μm for each laser, assuming identical beams. Taking the measured saturation with increasing power into account, the Rydberg volume diameters in our experiment are 11.6(4) μm for $49s$ and 16.3(5) μm for $41d$. Without assuming identical beams, the convolution of the two saturated Rydberg volumes (relevant for the experiment) has a full width of less than 23(1) μm. Because of the finite temperature, the diameter of the cylinders increases at most 2 μm in 25 μs.

For the interpretation of the data, we simulated the populations in each state by performing a fully quantum calculation with a limited number of atoms fixed in space. The matrix elements were computed using standard angular momentum algebra and numerical integration for the radial matrix elements. We used the energy levels of Ref. [24] to determine the radial functions needed for the matrix elements. No adjustments were made to get better agreement with the measurements. We randomly placed 25 atoms in each cigar-shaped ellipsoid (Gaussian in 3D) and performed a series of calculations starting with one randomly picked $49s$ atom. We added neighboring atoms in the calculation until the time dependent probability for the $49s \rightarrow 49p$ transition converged. We obtained good results with two $49s$ atoms and the two nearest $41d$ atoms, which are depicted in the figures; full convergence was obtained with one additional $41d$ atom. This demonstrates that many-body effects are important. Adding more electronic energy levels per atom or adding atoms initially in the $42p$ or $43p$ state slightly slowed down the transition times ($\sim20\%$).

As a first experiment we monitored the $49p$ fraction $N_{49p}/(N_{49s} + N_{49p})$, resulting from the resonant dipole-dipole interaction, after 10 μs as a function of the applied static electric field. The measurements performed with beam separations between 21 and 51 μm are depicted in Fig. 2. Two resonances can be seen, due to a small difference in the Stark shift of the $49p_{3/2}|m_j|$ states. At the field $F_1(F_2)$, $|m_j| = \frac{1}{2}(\frac{3}{2})$ is resonant. The $41d_{3/2}$ splitting is not visible, because only $|m_j| = \frac{1}{2}$ is excited by the laser. The field values have a systematic error of 2%, due to the uncertainty in the effective plate distance. The calculated resonances fit within this error, confirming that the creation

of $49p$ in the $49s$ volume requires the tuning into resonance with the transition in the adjacent $41d$ volume. For the top axis a conversion of 127 MHz/(V/cm) is used, based on the calculated difference of the total polarizabilities of the initial and final states.

It is clearly visible in Fig. 2 that the resonance peaks become higher and broader as the distance between the foci is reduced [FWHM are 18(2), 20(1), 29(1), and 29(1) mV/cm]. This is consistent with the notion that the dipole-dipole interaction [Eq. (2)] gets stronger with shorter distance. These features are also reproduced in the simulations. However, the widths of the calculated resonance peaks are much narrower than observed in the experiment. This is mainly due to the magnetic field of the MOT (~1.4 MHz). It will further be discussed in connection with Fig. 4, as well as the origin of the background of 0.1. The increasing background at shorter distance, visible in simulation and measurement, is due to an increase of overlap between the Rydberg volumes, as well as presumably many-body effects.

To investigate the distance dependence of the interaction, we tuned the field to each of the resonances and measured the transferred fraction after 10 μs as a function of the separation (Fig. 3). The most important result in this figure is that a range of distances exists, where the overlap of the lasers vanishes, while the interaction is still clearly present. This demonstrates dipole-dipole energy transfer between Rydberg atoms in separate volumes.

Figure 3 also shows simulations of the experiment. The effective range of interaction is well reconstructed, but slightly overestimated in the calculation. The inset shows
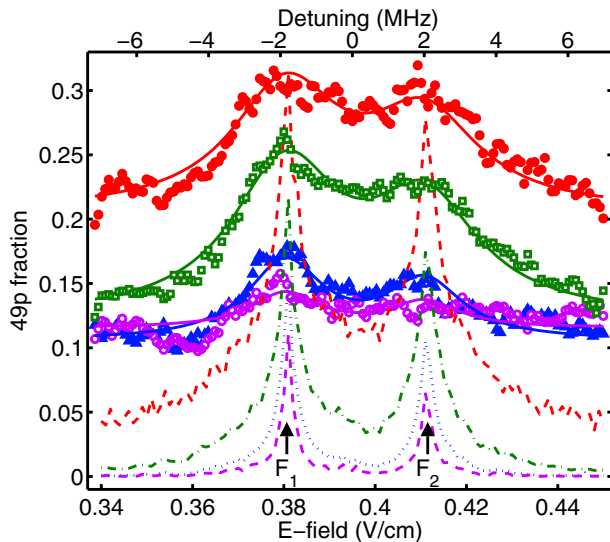
that the wings of the data follow a d^{-5} behavior, as expected. A striking discrepancy with the simulation is that the experimental signal decreases where the beams overlap. This is because nonresonant processes take place in the high density $41d$ beam, reducing the number of $49s$ atoms from 12.5(2.5) to 10(2); we particularly observe 4(1) atoms in the $47p$ state, but possibly Penning ionization occurs as well [25]. Besides, there are 5(1) $44d$ atoms due to the two-laser excitation. Within the accuracy of the experiment there is no significant difference between the resonance F_1 (blue ●) and the resonance F_2 (green □). The asymmetry of the measured curve might be due to a deviation from a Gaussian of the laser beam profiles or a decrease in the density for positive positions (~10%).

Next we will discuss the main result in this Letter, the temporal evolution of the interaction. In Fig. 4 the evolution of the $49p$ fraction is measured for various beam separations with the field tuned to the resonance F_1. The figure clearly shows that the rate of transfer slows down for larger distance, but even at a 50 μm separation an appreciable transfer is observed. The rates slow down because the interaction strength decreases strongly with distance [Eq. (2)]. Quantum beat oscillations, which are expected on the basis of the coherent coupling between atoms, are not observed. A spread in distances of the interacting atoms, and hence a spread in interaction strength, causes dephasing of these oscillations. The transition rate $1/\tau$ in the inset is based on the time τ where the measured $49p$ fraction has reached 0.17. It is plotted versus distance, slightly corrected for the finite cylinder width. The data points nicely fit the scaling law $d^{-5/2}$. The minor deviation might be related to the different asymptotes of the curves.
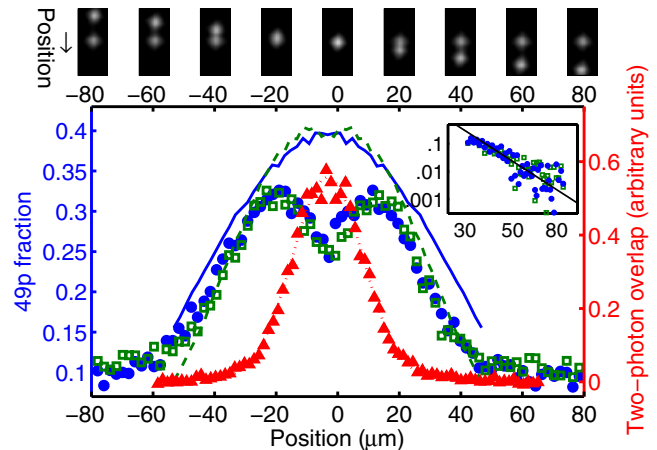

FIG. 2 (color online). The $49p$ fraction after 10 μs as a function of electric field for different beam separations: red ● 21, green □ 31, blue ▲ 41, and purple ○ 51 μm. Solid lines are Lorentzian fits. Red dashed (20 μm), green dash-dotted (30 μm), blue dotted (40 μm), and purple dashed (50 μm) lines are simulations. F_1 (0.38 V/cm) and F_2 (0.41 V/cm) are the resonances. The top axis depicts a relative energy scale.

FIG. 3 (color online). The $49p$ fraction after 10 μs as a function of the position of the $49s$ beam at the resonances F_1 (blue ●) and F_2 (green □). Blue solid (F_1) and green dashed (F_2) lines are simulations. The measured beam overlap (red ▲) is fitted to a Gaussian (red dotted line). CCD pictures of the laser foci above the graph correspond to the horizontal axis tick marks. The log-log plot inset depicts the wings of the data together with a fit to d^{-5}.

Figure 4 also shows results of the simulations. The curves reproduce the experimental data in a qualitative way, but the calculated growth rate is slightly higher and the final production is somewhat different. An important factor to note is that temporal fluctuations in the electric field, which are fast with respect to the dipole-dipole interaction rate, will slow down the transfer rate. These fluctuations diabatically detune an interacting atom pair in and out of resonance, thereby reducing the fraction of time during which the interaction actually takes place. Indeed, in early runs of the experiment, where the high-frequency noise level of the field generated by the field plates was 10 rather than 2 mV/cm, the observed transfer times were a factor of 2.8(5) longer. Moving ions in the MOT cloud might also contribute to electrical field noise. Furthermore, the initially present $42p$ and $43p$ atoms also slow down the transfer rate, as indicated by the simulations.

The final $49p$ fraction is not 50%, which one would expect on the basis of binary interaction. This reduced transfer is due to time-independent broadening effects, mainly the magnetic field (see also Fig. 2). However, since the transferred fraction is also below 50% in the simulations, it is probable that also many-body effects play a role. The main process can be accompanied by interactions between the initial $49s$ and the reaction product $49p$, as well as between $41d$ and $42p$. These processes are always resonant and occur within a single cylinder. Spurious processes within the $49s$ beam can be observed when the $41d$ laser is turned off, depicted as purple $\triangle$ in Fig. 4. This is

mainly due to black body radiation; the transition from $49s$ to $49p$ has a rate of 6.7 kHz [23], but possibly also nonresonant two-body processes play a role.

Up till now distance dependence of dipole-dipole interactions in Rydberg atoms has only been measured indirectly by varying the density. Here, we have taken the next step by having interaction between atoms in different volumes at a well defined separation. This is remarkable since an interaction is measured between two mesoscopic gaseous systems at a macroscopic distance. We map the interaction by varying the electric field, mutual separation, and interaction time, and our data fit the simulations presented here as well as a straightforward scaling law. The distance restriction is not strong enough to show the coherence of the underlying processes. Furthermore, because of the fact that only interactions at large distances play a role, this experiment is more sensitive to many-body interactions and external fields. When this approach is combined with position-sensitive measurements [22], it allows for many variations with more complexity and/or reduced dimensionality and hence coherent evolution.
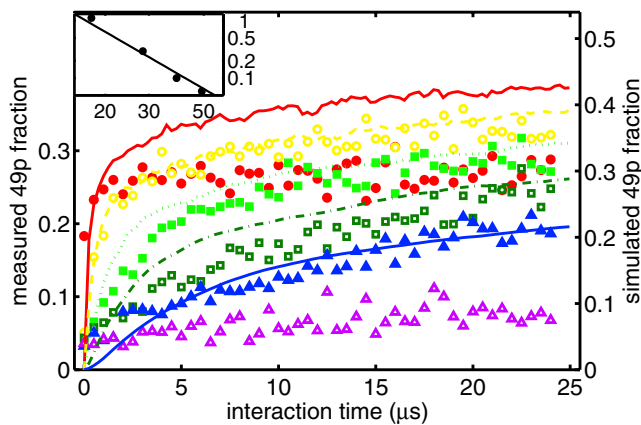
FIG. 4 (color online).   The growth of the $49p$ fraction for different beam separations, measured data are red ● 0, yellow ○ 20, green ■ 30, dark green □ 40, blue ▲ 50 μm, and purple △ with only $49s$ atoms created (or ∞ separation). The interaction time is controlled by varying the delay between the laser excitation and the field ionizing ramp. The simulations are depicted as solid red (0 μm), dashed yellow (20 μm), dotted green (30 μm), dash-dotted dark green (40 μm), and solid blue (50 μm) lines. The left axis refers to the measured data, and the right axis to the simulations. The inset shows a log-log plot of the transfer rate $1/\tau$ in MHz versus the effective distance together with a fit to $d^{-5/2}$.

*heuvell@science.uva.nl
[1] A. van Oijen *et al.*, Science **285**, 400 (1999).
[2] J. L. Herek *et al.*, Nature (London) **417**, 533 (2002).
[3] T. Förster, Ann. Phys. **2**, 55 (1948).
[4] E. A. Jares-Erijman *et al.*, Nat. Biotechnol. **21**, 1387 (2003).
[5] M. Quinten *et al.*, Opt. Lett. **23**, 1331 (1998).
[6] M. L. Brongersma *et al.*, Phys. Rev. B **62**, R16356 (2000).
[7] J. V. Hernández *et al.*, J. Phys. Chem. B **109**, 15808 (2005).
[8] A. F. Koenderink *et al.*, Phys. Rev. B **74**, 033402 (2006).
[9] D. Jaksch *et al.*, Phys. Rev. Lett. **85**, 2208 (2000).
[10] M. D. Lukin *et al.*, Phys. Rev. Lett. **87**, 037901 (2001).
[11] F. Robicheaux *et al.*, Phys. Rev. A **70**, 042703 (2004).
[12] M. Saffman *et al.*, Phys. Rev. A **72**, 042302 (2005).
[13] G. Burkard *et al.*, Phys. Rev. B **74**, 041307(R) (2006).
[14] C. Hettich *et al.*, Science **298**, 385 (2002).
[15] W. R. Anderson *et al.*, Phys. Rev. Lett. **80**, 249 (1998).
[16] K. Afrousheh *et al.*, Phys. Rev. Lett. **93**, 233001 (2004).
[17] T. J. Carroll *et al.*, Phys. Rev. Lett. **93**, 153001 (2004).
[18] T. J. Carroll *et al.*, Phys. Rev. A **73**, 032725 (2006).
[19] W. Li *et al.*, Phys. Rev. Lett. **94**, 173001 (2005).
[20] T. Vogt *et al.*, Phys. Rev. Lett. **97**, 083003 (2006).
[21] S. Westermann *et al.*, Eur. Phys. J. D **40**, 37 (2006).
[22] C. S. E. van Ditzhuijzen *et al.*, Eur. Phys. J. D **40**, 13 (2006).
[23] T. F. Gallagher, *Rydberg Atoms* (Cambridge University Press, Cambridge, 1994).
[24] W. Li *et al.*, Phys. Rev. A **67**, 052502 (2003).
[25] A. Walz-Flannigan *et al.*, Phys. Rev. A **69**, 063405 (2004).